USING EARTHQUAKE CLUSTERS TO IDENTIFY FRACTURE ZONES AT PUNA GEOTHERMAL FILED, HAWAII

A Lucas, C Kenedi, E Shalev and P Malin
Institute of Earth Science and Engineering, University of Auckland, Auckland, New Zealand
e-mail: a.lucas@auckland.ac.nz

ABSTRACT

The actively producing Puna geothermal system (PGS) is located on the Kilauea East Rift Zone (ERZ), Hawaii. In the Puna area the rift trend is identified as NE-SW from surface expressions of normal faulting, at PGS the rift offsets in a left step. The spread of earthquake locations follows the rift trend. Double difference (DD) relocation of all earthquakes identified one large cluster but could not conclusively identify trends within the cluster. For five stations out of the six, where shear wave splitting was observed, the dominant polarization direction was rift parallel. Two of the five stations also showed a smaller rift perpendicular signal. The shear wave splitting time delays indicate that fracture density is higher at the PGS compared to the surrounding ERZ. Correlation co-efficient clustering was used to identify clusters based on similar earthquake waveforms. In total, 40 localized clusters containing ten or more events were identified. Most of the clusters had linear features when their locations were plotted and were further enhanced by DD relocation. The concentration of individual linear features was higher in the PGS than the surrounding ERZ. Mapping of the linear features showed that a number of the larger features ran rift parallel. However a large number of rift perpendicular features were also identified. We assume that events occurring on the same fracture zone have similar source mechanisms and thus similar waveforms. It is concluded that the linear features identified by earthquake clustering are fracture zones. The orientation and concentration of the fracture zones is consistent with that of the shear wave splitting polarizations.

Keywords: microseismicity, shear wave splitting, fracture zones, focal mechanisms

1. INTRODUCTION

The Puna geothermal field is located in the lower half of the Kilauea Volcano East Rift Zone (KERZ), Big Island, Hawaii. The lower KERZ trends SW-NE and is defined by normal faulting with similarly trending strike (**R.B. Moore and F.A. Trusdell, (1991)**). In the Puna region there is no surface expression of rift perpendicular faulting. Local eruptive features include cones, craters, and fissures, which often form linear trends striking parallel to the rift. The cones and fissures are often associated with lava flows, including extensive resurfacing in 1955 and 1960. In Puna, the surface expression of the rift system offsets in a left step in which the geothermal system is located (**C.L Kenedi. (2010)**). Locally there is no surface discharge of geothermal fluids, but hot springs emerge at the coastline, at approximately 200 m lower elevation.

The geothermal system is currently being tapped by a 30 MW power station, operated by Puna Geothermal Venture (PGV). The distinctive shape of the PGV lease boundary will be used as a point of reference for all figures in this paper. The rift offset is thought to cut through the lease boundary.

2. METHODS

Since 2006 seismicity in the PGV region has been recorded by an eight component borehole seismometer network. The network consists of five stations with 2-Hz geophones and three with 4.5-Hz geophones. The instrument depths range from 24 – 210 m. Data are continuously recorded at a rate of 200 samples/sec. This paper discusses the period 20 June 2006 to 19 January 2009, during which time 6162 earthquake events were located. A calibrated (through events co-located with the Hawaiian Volcano Observatory) magnitude algorithm showed that the lower limit of this network is approximately magnitude -0.2.Over the recording period significant changes in the daily microseismicity rate occurred. In Nov 2006 the rate changed from ~8 events/day to ~20 events/day; in Aug 2007 the rate dropped down to ~4 events/day. The reason for this variation is not clear. When the network was installed, the power station had been producing electricity for 13 years, so no indication of natural vs. induced rate of seismicity is possible. Other seismic networks in the area, including an pre-production test survey (**P. Cooper, and M. Dustman (1995)**), have been surface-based and therefore unable to detect the low magnitude seismicity seen on the current array.

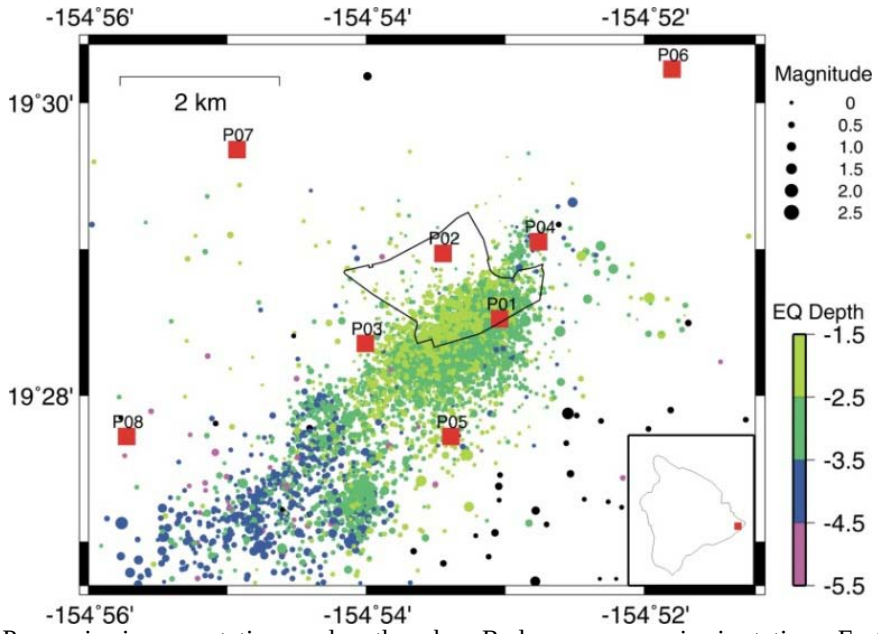

Fig. 1 Map views of Puna seismic array stations and earthquakes. Red squares are seismic stations. Earthquake locations are marked by dots colored according to depth. The size of the dots indicates the magnitude, ranging from M-0.2 to M2.0.

Microearthquakes were located initially using the USGS Fortran program, Hypoinverse 72 (REF),. The distribution of seismicity follows the trend of the rift system (Figure 1). In the area of the rift offset, microseismicity is very dense; with the density decreasing along rift to the SW. Very few events occur to the NE of the rift offset, and further to the NE is a zone that is aseismic for the duration of recording. There appears to be an N-S oriented boundary to seismicity.

The depth of seismicity varies relative to position along the rift (Figure 1). In the region of the rift offset, earthquakes are concentrated over a range of depths from 1.5 - 3 km. Earthquake depths increase to 3.5 – 4 km SW of the offset and to >5.5 km to the SE. Earthquakes to the north of the rift are shallower than those the south.

The earthquake magnitude statistics closely follow a Gutenberg-Richter power law style relationship (**B Gutenberg and CF Richter (1954)**). At Puna the B value is 1.285, meaning that for every drop of one level of magnitude there is a >25 fold increase in the number of observed earthquakes. The largest local earthquakes observed were approximately M 2.5. There appears to be no spatial relationship in the distribution of earthquake magnitudes other than depth.

Double difference relocation (both with and without correlation) of the entire data set was attempted using the HypoD D code of **Waldhauser and Ellsworth (2000)** and **Waldhauser and Ellsworth (2002)**. In all the different evaluations with varying clustering parameters HypoDD never identified more than 10 separate clusters. For the purposes of this paper we define an earthquake cluster as a group of earthquakes (numbering 2 or larger) linked through a common attribute. The best relocation (based on RMS residual) showed some possible structures but with insufficient confidence to draw a conclusion.

3. EARTHQUAKE CLUSTERING

As the results of a double difference relocation of the microseismic events proved inconclusive, a waveform correlation method was applied (**H. Maurer and N. Deichmann, (1995)**, **W.L. Ellsworth and J. Frechet, (1984)** and **S.I. Pytharouli, etal (2011))**. Central to this method is the assumption that earthquakes that occur close together on the same fracture zone will have similar waveforms. This is based on two observations; firstly earthquakes occurring on the same fracture zone are likely to have similar source mechanisms. Secondly, because the events have similar paths to the stations, the effects of the transmission medium will be the same.

All the earthquakes were ordered in terms of origin time and assigned an identification number from 1 to 6162 (the first earthquake recorded =1). The correlation coefficient was calculated for each microseismic event compared to all other

events in the cluster. Each correlation was done separately on a window of data around the P (1 sec window) and S (2 sec window) hand-picked arrival times. To improve the correlation both windows were started 0.2 sec in front of the pick. If the P-window ended after the arrival of the S-wave then the waveform was truncated at the S pick and padded out to one second.

Where the correlation coefficient exceeded 0.75 for either the P or S wave a doublet was identified (see Figure 3). This information was stored in a matrix [x,y] in which x and y vary between 1 and 6162. The value of any point inside the matrix (x,y) indicates if the correlation of events x and y is above (1) or below (0) the correlation threshold. If x and y are equal the correlation is always one (diagonal components =1). The correlation of x and y is the same as y and x, making the matrix symmetric around the diagonal axis. This symmetry means that only half the components of the matrix need to be calculated, thereby speeding up a lengthy computation.

The cluster correlation matrix indicates which events are linked. To further enhance this relationship a modified network correlation matrix is derived directly using the procedure defined in. This procedure denotes a correlation if the normalized scalar product is above 0.4. If event x correlates with y1, but it also correlates with y2, then y1 and y2 must also correlate. Thus it follows that events y1, y2 and x form a cluster. By using a dot product relationship, clusters of events organize out of the matrix.

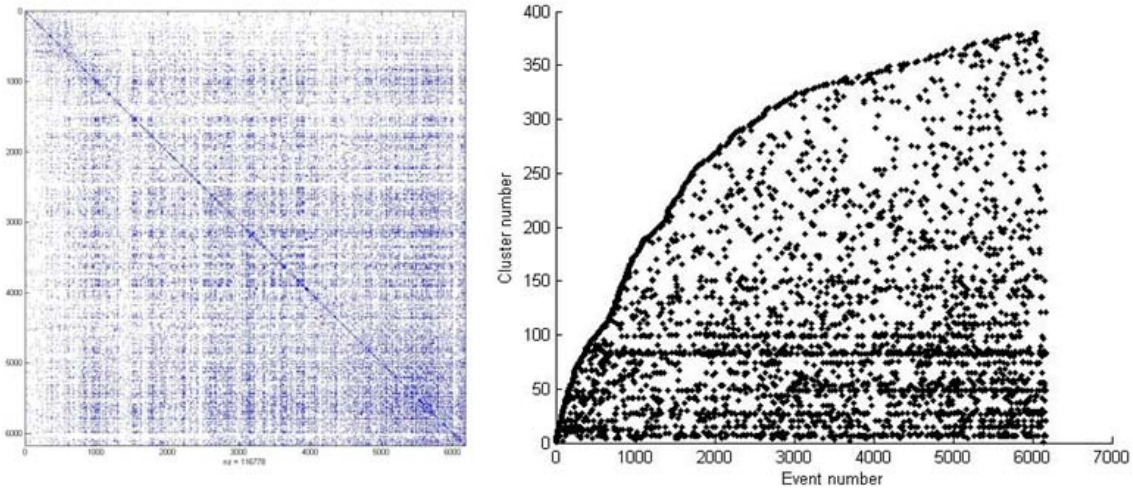

Fig.2 Matrix representation of the cluster correlation matrix (2a left) and the resultant cluster number plot (2b right). The cluster number (1:6162) is ordered consecutively over the recording period, i.e. event 1 is the first event recoded and event 6162 the last.

This process identified more than 350 different clusters, but most of the clusters contained 10 or fewer events. In total 80 clusters consisted of more than 10 events. These clusters were relocated using the standard double difference algorithm (HypoDD). Given the large number of clusters only the catalog method was used in this relocation.

The structure of individual clusters varies; some clusters are planar, while the largest is spherical (and located in the area of production).Using principal component analysis, planes were fit to each of the clusters (**J.E. Jackson (1991))**. Outlying events contained in some of the clusters significantly influenced the result of this fitting. Generally the clusters were tightly grouped with outlying events often separated by some distance. Therefore outliers were identified by distance (> 0.6 km) from the mean cluster location and excluded from the fitting process. The averaged residual distance between the plane and events was used to identify well-fitting planes. A RMS residual of less 0.001 was chosen as the limit that defined a high quality fit. For visualization purposes the planes and the corresponding earthquakes were plotted both in 3D and as slices through the planes at varying depths. In taking depth slices the intersection of the plane and the slice (a line along the strike of the plane) were calculated and plotted (Figure 4). The length of the plotted line was taken from the size of the cluster in the direction the line was trending.

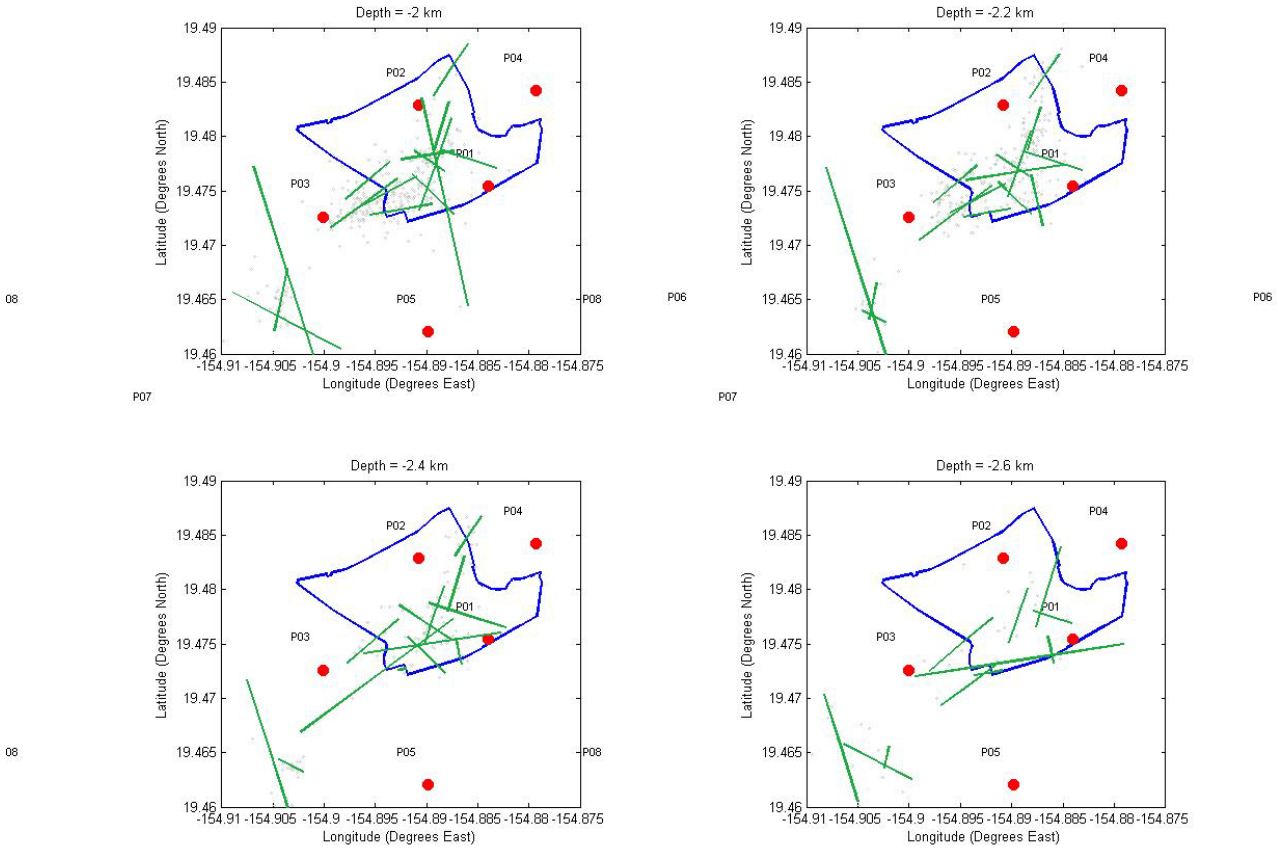

Fig.3 Depth slices of the intersection of the fracture plane at a set depth (green). The length of the lines depends on the size of the cluster at that depth.

It is hard to gauge the true accuracy of the fitted plane as the resultant error is only in the fitting to the points. As the points have varying errors it would be preferable to include them in the plane fitting process (currently being worked on). The dip of the fitted planes is less accurate than the strike because the earthquake location accuracy is almost always worse vertically than horizontally.

A number of the fitted planes can be observed to have similar orientations, in particular the set which forms a line trending SW from the NE corner of the PGV lease boundary (Figure 3). It is possible that two different sets of earthquakes used to generate two different planes occurred on the same fracture system. There are several mechanisms that may have resulted in this. The different clusters may be dominated by earthquakes occurring at different times, possibly resulting in different source mechanisms. Also possible is that the source-receiver path may change significantly enough along the fracture zone that events get classified into different groups.

At Puna we see that within a single cluster, the earthquakes are spread out over the entire recording period, however in most clusters show a varying rate of earthquake occurrence. This is shown by the cluster numbering system and the cluster correlation matrix (refer to Figure (2)). Currently no research into the mechanisms behind this variation has been conducted.

4. FOCAL MECHANISMS

Calculations of the focal mechanisms for all earthquakes were attempted. The HASH (**J.L. Hardebeck and P.M. Shearer (2003)** & **J.L. Hardebeck and P.M. Shearer (2003)**) code uses both the orientation of the P-wave first break and the ratio of P and S wave amplitudes At Puna the limited number of stations (8) significantly impacts the number and accuracy of

focal mechanisms calculated. Mechanisms can be calculated most accurately at the center of the array. Even with the large number of earthquakes occurring in this area, a total of only 36 focal mechanisms were found with a quality factor greater than D. Out of this number, two with qualities of B were identified and none occurred with an A. However this analysis was only performed on events up to the beginning of 2008. The goal was to identify mechanisms for earthquakes occurring as part of a cluster and compare the fault plane solution to that of the fitted plane of the cluster, but the number of mechanisms limited our ability to do this. Therefore all focal mechanisms were plotted to allow comparison between the two methods.

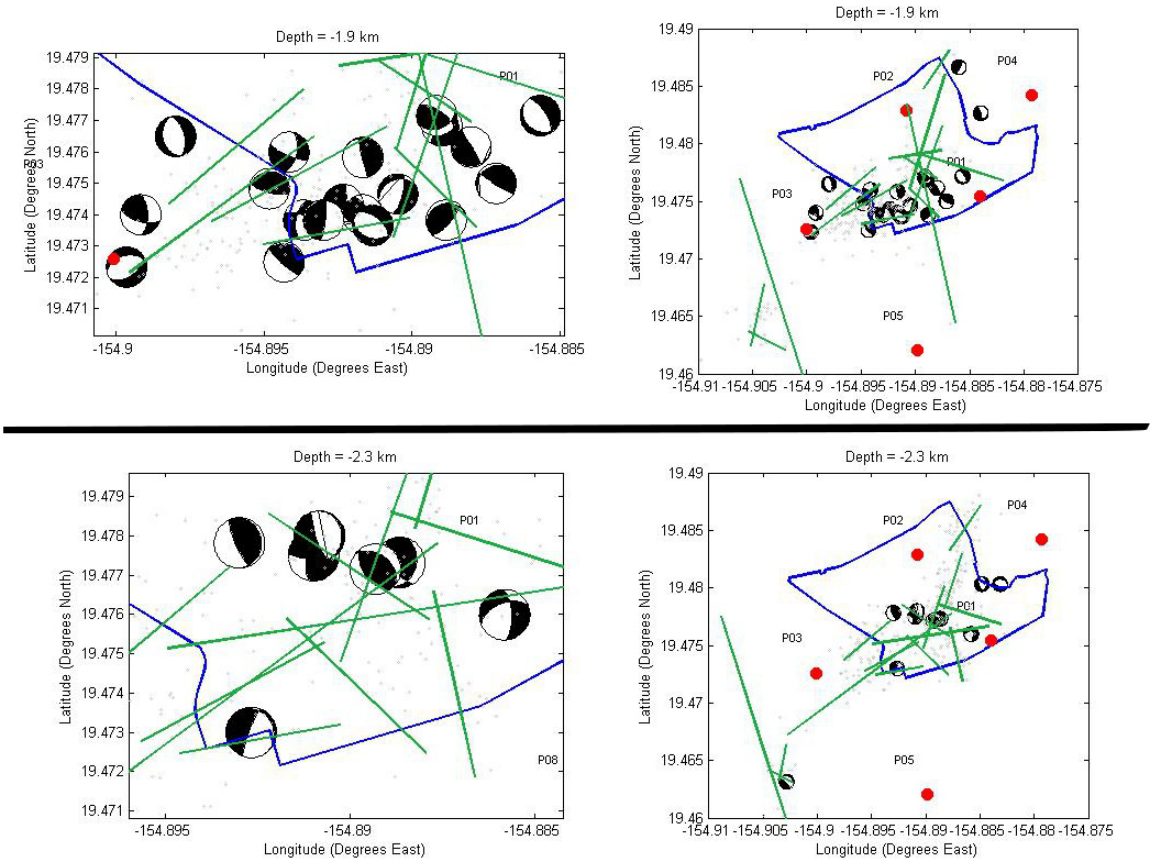

Fig.4 Depth slices of the intersection of the plane at a set depth (green). The length of the lines depends on the size of the cluster at that depth. The two plots on the left are expanded sections (at the same depth) of the right hand plots.

In the area of the PGV lease the focal mechanisms are dominantly normal or reverse type faulting (Figure 5). The fault planes are either near vertical or horizontal; given the tectonic situation it is much more likely that the faults are near vertical. Strike slip and oblique slip form the minority of events. The strike of all the events located in the PGV lease varies significantly over short distances. The solution for events well outside the boundary is insufficiently constrained, so the mechanisms are not accurately calculated. However it was possible to calculate one event in the NE of the offset and one to the SW (Figure 4).

5. SHEAR WAVE SPLITTING

Shear wave splitting (SWS) occurs when a shear wave is transmitted through seismically anisotropic rock. One form of anisotropy relates to the crystalline properties of the rock (**D.L. Abt and K.M. Fischer (2008)**) and the other to parallel, aligned fluid-filled fractures (**D.F. Winterstein and M.A. Meadows (1991)**). In geothermal systems (where SWS is often observed) it is commonly assumed that the second method is the dominant cause of SWS (**C. Tang, J.A. Rial and J.M. Lees (2008)** and **M. Lou and J.A. Rial (1997)**).

During the transmission of the shear wave, the anisotropic medium polarizes the wave; the “fast” wave is orientated in the fast direction of the anisotropy and the “slow” wave in the slow direction. The time delay between the fast and slow waves

can be used to infer the degree of anisotropy, and the orientation (relative to north) of the fast arrival is used to indicate the orientation of the anisotropy (**S. Crampin and S. Peacock (2005)**).

At Puna the dominant orientation is observed to be rift parallel (Figure 5). The exception is at station P04 (at the north end of the lease and on the immediate NE side of the rift offset), which displays an N-S orientation. The southern stations P01 and P05 show a bimodal orientation: The dominant direction is rift parallel, but there is a secondary rift perpendicular orientation.

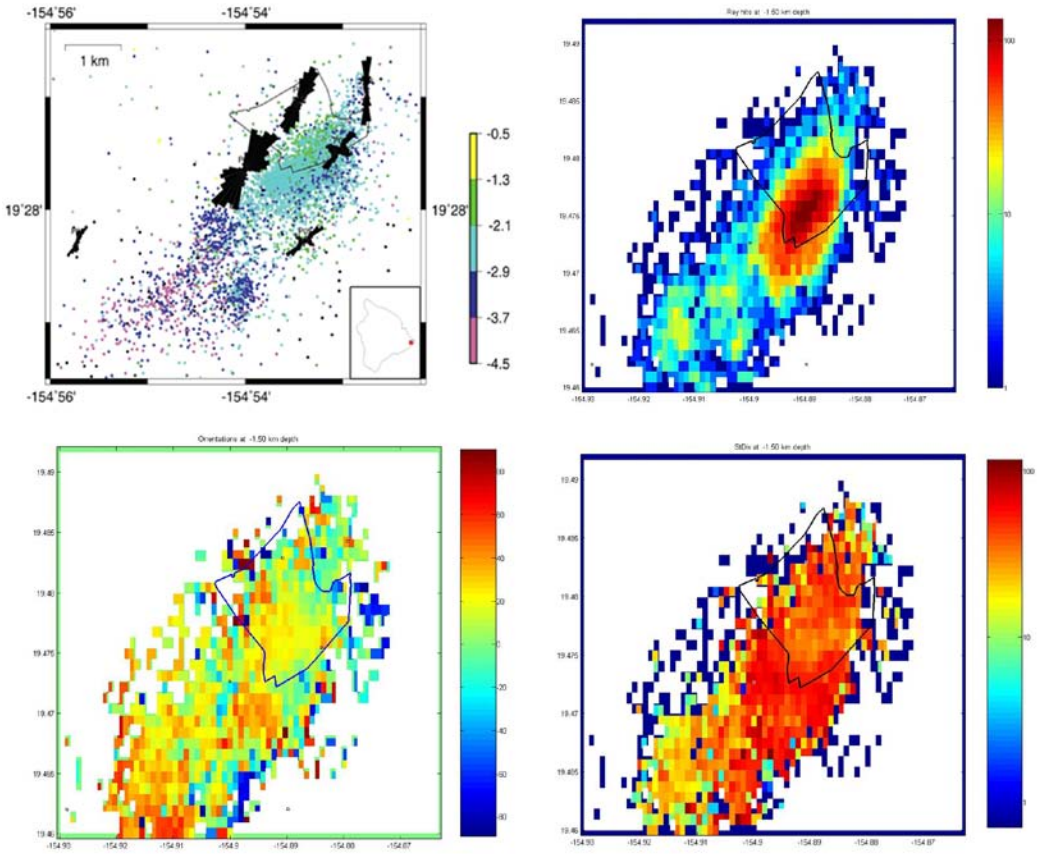

Fig.5 The SWS orientations (top left) observed at Puna, in the background are the all the earthquakes located. The hit plot (top right) at a depth of 1.5 km, note the color scale is exponential. The SWS orientation (bottom left) at a depth of 1.5 km and the standard deviation of the orientation (bottom right).

It is possible to invert directly for shear wave splitting time delays because the process is linear REF. Orientations act in a non-linear fashion and therefore currently cannot directly inverted for. However it is possible to map the orientations. This is a statistical process that assumes that the observed orientation must occur at some point along the ray path.

The study area is separated into a 3D grid of cubes with sides 0.1 km long. The earthquakes and stations are located within this grid. For every shear wave splitting observation the station-earthquake pairs are identified and a straight line ray path defined. At every cube in the grid through which a ray passes, the observed orientation is binned. This is done for all station-earthquake pairs for which SWS is observed. The result is a data volume containing the orientations of all rays passing through each location. The standard deviation of each bin indicates the variation. The hit plot indicates the number of rays passing through each bin. In areas where the standard deviation is low and the hit number is high, it follows that the average of the orientations in the bin will indicate the geological situation. Conversely if the hit count is low then the average of the orientations will not be confidently useful. If the standard deviation is high then a large range of orientations is being averaged and caution is needed in interpreting the average.

This method of mapping shear wave splitting orientations only supplies information about the transmission medium. At Puna the depth (average 3km) and lateral spread (within the rift) limits the scope of the map. This is a different area than that covered by the earthquake clustering and focal mechanisms calculated earlier. There is however some degree of overlap; we see focal mechanisms and earthquake locations from 1.5 to 3km and accurate maps from 0 to 2km. It is also plausible that a structure occurring at 2-3km would extend up to 1km deep. Therefore it is foreseeable that structures identified through clustering may also be seen in the SWS mapping.

The orientations in the southern part of the PGV lease vary around 20-40 degrees with a standard deviation of 30-40 degrees. In comparison the orientations in the NW of the PGV lease vary around 0- -20 degrees with a high standard deviation of 40-50 degrees. In both of these regions the hit count is high (between 10 and 100 hits) indicating a moderate degree of accuracy. Down rift, to the SW from the lease, the standard deviation drops and the orientation consistently is around 45 degrees, but the hit count in this region is low (between 1 and 10). Because SWS only occurs where parallel fluid filled fractures are present, the lack of a large signal does not indicate un-fractured rock, just that any fractures present do not meet the SWS requirements. Some of the seismically active fracture systems identified earlier may not meet these requirements and therefore produce no SWS.

4. DISCUSSION

As Puna is a producing geothermal system there has been ongoing drilling over a number of years. The main production of the area occurs in the SW corner of the lease. In this area a number of rift parallel faults are encountered. Two dominant rift parallel structures form the main productive zones. The northern structure is found to dip to the south and the southern structure to the north.

There are results in each of the three data sets which correlate. The focal mechanisms in the NE and SW of the offset strongly correlate with fracture zones computed through earthquake clustering. In the region of the offset both focal mechanisms and clustering show overlapping trends. Therefore it is hard to associate individual focal mechanisms with fracture zones. These correlations also carry through to the SWS mapping. However the standard deviation indicates a high error in the SWS orientation result.

These results are interpreted to show that three different orientations of fracturing are present in the region of the Puna rift offset. The dominant orientation is rift parallel (45 degrees from north) and is concentrated in the southern end (extending SW) of the lease. These fractures zones contain near vertical, fluid filled normal and reverse faults. Fractures of this type have been drilled and are producing hydrothermal fluid. If these fractures extend NE through to the eastern side of the lease they are not seismic active and therefore have not been mapped.

The second type of fracture orientation observed is 10-20 degrees (relative to north). These fractures cut across the lease from the south to the north and are found to be near vertical. There is also some evidence that fractures of this orientation exist in the SW edge of the study region, however it must be noted that accuracy in this region is low. Very few focal mechanisms are found in the region of these fractures. The few that can be calculated show normal or vertical faulting.

The final type of fracture orientation observed is -10 to -45 degrees. This orientation is the least common direction observed. It occurs solely in the southern end of the lease and possibly at the south eastern end of the study area. There is evidence that fractures of this orientation show SWS implying that they are fluid filled. However the SWS related to this fracture orientation is a small percentage of the total observed SWS.

5. SUMMARY

Three different fracture zone orientations are described in the area of the PGV lease, only one of these orientations (rift parallel) is observed at the surface. Two of the orientations have an associated shear wave splitting signature and are therefore likely to be fluid filled. All three orientations are observed in the focal mechanisms generated from the earthquakes used to derive the fracture zones

REFERENCES

D.L. Abt and K.M. Fischer (2008) Resolving three-dimensional anisotropic structure with shear wave splitting tomography, *Geophys. J. Int.* 173, 859–886

P. Cooper, and M. Dustman (1995) Field studies of seismic anisotropy in the shallow crust of the Puna Geothermal Field, Hawaii. *Seismological Research Letters.* 66:2.

S. Crampin and S. Peacock (2005) A review of shear-wave splitting in the compliant crack-critical anisotropic Earth, *Wave Motion*, 41, 59–77

B Gutenberg and CF Richter (1954) Seismicity of the earth and associated phenomena, 2nd edn. Princeton University Press, Princeton

J.L. Hardebeck and P.M. Shearer (2003) A New Method for Determining First-Motion Focal Mechanisms, *Bull. Seis. Soc. America*, 92, 6, 2264-2276

J.L. Hardebeck and P.M. Shearer (2003) Using S/P Amplitude Ratios to Constrain the Focal Mechanisms of Small Earthquakes, *Bull. Seis. Soc. America*, 93, 6, 2434-2444

J.E. Jackson (1991) A User's Guide to Principal Components, John Wiley and Sons

C.L Kenedi. (2010) Fractures, Faults, and Hydrothermal Systems of Puna, Hawaii, and Montserrat, Lesser Antilles. PhD Dissertation, Duke University. 103 pp.

M. Lou and J.A. Rial (1997) Characterization of geothermal reservoir crack patterns using shear-wave splitting. *Geophysics*, 62, 2, 487-494

H. Maurer and N. Deichmann, (1995) Microearthquake cluster detection based on waveform similarities, with application to the western Swiss Alps, *Geophys. J. Int.* 123, 588-600,

R.B. Moore and F.A. Trusdell, (1991) Geologic map of the Lower East Rift Zone of Kilauea Volcano, Hawaii, U.S. *Geological Survey Miscellaneous investigations series*, map I-2225.

G. Poupinet, W.L. Ellsworth and J. Frechet, (1984) Monitoring velocity variations in the crust using earthquake doublets: an application to the Calaveras fault, California (USA). *Journal of Geophysical Research*, 86, B7, 5719-5731

S.I. Pytharouli, R.J. Lunn, Z.K. Shipton, J.D. Kirkpatrick and A.F. do Nascimento (2011) Microseismicity illuminates open fractures in the shallow crust, *Geophysical Research Letters*, 38, L02402

J.A. Rial , M. Elkibbi and M. Yang (2005) Shear-wave splitting as a tool for the characterization of geothermal fractured reservoirs: lessons learned, *Geothermics*, 34, 365-385

C. Tang, J.A. Rial and J.M. Lees (2008) Seismic imaging of the geothermal field at Krafla, Iceland using shear-wave splitting, *Journal of Volcanology and Geothermal Research,* 176, 315-324

F. Waldhauser and W. Ellsworth (2000) A Double difference earthquake location algorithim: method and application to the northern Hayward fault, California, *Bull. Seis. Soc. America*, 90, 6, 1353-1368

F. Waldhauser and W. Ellsworth (2002) Fault structure and mechanics of the Hayward Fault, California from double-difference earthquake locations,

D.F. Winterstein and M.A. Meadows (1991) Shear-wave polarizations and subsurface stress directions at Lost Hills field, *Geophysics*, 56, 9, 1331-1348